

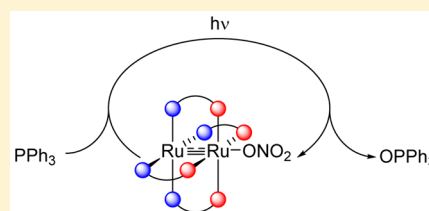
# A Synthetic Oxygen Atom Transfer Photocycle from a Diruthenium Oxyanion Complex

Amanda R. Corcos, József S. Pap,<sup>‡</sup> Tzuhsiung Yang, and John F. Berry\*

Department of Chemistry, University of Wisconsin—Madison, 1101 University Avenue, Madison, Wisconsin 53706, United States

**S** Supporting Information

**ABSTRACT:** Three new diruthenium oxyanion complexes have been prepared, crystallographically characterized, and screened for their potential to photochemically unmask a reactive Ru—Ru=O intermediate. The most promising candidate, Ru<sub>2</sub>(chp)<sub>4</sub>ONO<sub>2</sub> (**4**, chp = 6-chloro-2-hydroxypyridinate), displays a set of signals centered around *m/z* = 733 amu in its MALDI-TOF mass spectrum, consistent with the formation of the [Ru<sub>2</sub>(chp)<sub>4</sub>O]<sup>+</sup> ([**6**]<sup>+</sup>) ion. These signals shift to 735 amu in **4**<sup>\*</sup>, which contains an <sup>18</sup>O-labeled nitrate. EPR spectroscopy and headspace GC-MS analysis indicate that NO<sub>2</sub><sup>\*</sup> is released upon photolysis of **4**, also consistent with the formation of **6**. Photolysis of **4** in CH<sub>2</sub>Cl<sub>2</sub> at room temperature in the presence of excess PPh<sub>3</sub> yields OPPh<sub>3</sub> in 173% yield; control experiments implicate **6**, NO<sub>2</sub><sup>\*</sup>, and free NO<sub>3</sub><sup>-</sup> as the active oxidants. Notably, Ru<sub>2</sub>(chp)<sub>4</sub>Cl (**3**) is recovered after photolysis. Since **3** is the direct precursor to **4**, the results described herein constitute the first example of a synthetic cycle for oxygen atom transfer that makes use of light to generate a putative metal oxo intermediate.

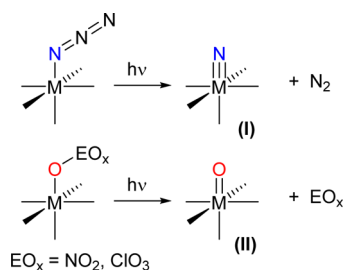


## INTRODUCTION

The use of light in chemical synthesis is a topic of significant current interest.<sup>1</sup> We<sup>2</sup> and others<sup>3</sup> have recently used light to access putative, highly reactive transition-metal-containing intermediates. The most well-known examples are metal nitride compounds (**I**), which can be photochemically accessed from metal azide precursors (Scheme 1).<sup>4</sup> Metal terminal oxo species

coordinated oxyanions, while Newcomb<sup>11</sup> and Bakac<sup>12</sup> have used flash photolysis to observe similar, highly reactive species. A major difficulty hindering the synthetic utility of this approach is the question of how to regenerate the M—OEO<sub>x</sub> precursor (Scheme 2). This transformation, shown with a

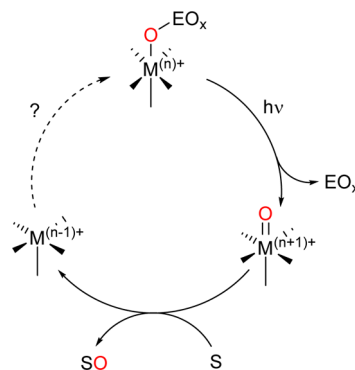
**Scheme 1. Formation of Mononuclear Metal Nitride and Oxo Species after Exposure of Metal Azides and Oxyanions to Light, Respectively**



(**II**) are related reactive intermediates that are of great importance for biological and synthetic oxidation reactions.<sup>5</sup> Typically, chemical or electrochemical redox reactions<sup>5a,6</sup> are used to access **II**, but here we probe the possibility of photochemically unmasking a highly reactive species **II**, as shown in the bottom of Scheme 1.

Important precedents for this work include the elimination of nitrite ion from an O= Ru—ONO<sub>2</sub> complex to produce a dioxo Ru species<sup>7</sup> and disproportionation of nitrite to form both Ru=O and Ru—NO complexes.<sup>8</sup> Furthermore, Suslick<sup>9</sup> and Vogler<sup>10</sup> have reported formation and reactivity of metal oxo species by photolytic cleavage of complexes with O-

**Scheme 2. Possible Stoichiometric Cycle Illustrating the Synthetic Limitations of Current Oxyanion Systems**



question mark in Scheme 2, is problematic because substrate (**S**) oxidation yields a coordinatively unsaturated metal complex that is reduced by one electron from the original M—OEO<sub>x</sub> species. Installation of OEO<sub>x</sub><sup>-</sup> with concomitant one-electron oxidation is problematic because the OEO<sub>x</sub><sup>-</sup> ions themselves can act as two-electron oxidants. We report here a solution to this problem that makes use of the properties of metal—metal bonded compounds.

Received: June 9, 2016

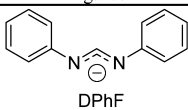
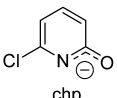
Published: July 13, 2016

We recently described the first examples of  $M-Ru=O$  species (in which  $M = Mo$  or  $W$ ), and we found them to display unusual reactivity.<sup>13</sup> Related  $Ru-Ru=O$  intermediates have recently been proposed to be important in sulfide oxygenation<sup>14</sup> and water oxidation<sup>15</sup> catalysis; furthermore,  $Ru_2(II/II)$  complexes have been shown to reversibly bind  $O_2$ .<sup>16</sup> Putative  $Ru-Ru=O$  species are highly reactive and have not been observed or isolated. Due to their important catalytic applications and our expertise in the chemistry of  $Ru-Ru\equiv N$  intermediates, we sought to use the photochemical methods outlined above to access  $Ru-Ru=O$  species in order to explore their fundamental reactivity. We also find the  $Ru-Ru=O$  species to be unstable, but it can nonetheless be utilized in a synthetic photocycle for oxygen atom transfer.

## RESULTS AND DISCUSSION

To date, only two discrete (non-polymeric)  $Ru_2$  compounds bearing axial oxyanionic ligands are known:  $Ru_2(DMBA)_4(ONO_2)_2$  ( $DMBA = N,N'$ -dimethylbenzamidinate),<sup>17</sup> which contains two  $\eta^1$ -coordinated nitrate ligands, and  $Ru_2(OAc)_4(ONO_2)(H_2O)$ ,<sup>18</sup> which forms polymeric chains upon loss of the aquo ligand. We are instead keen to explore whether a discrete, anhydrous mono-oxyanion complex with an  $Ru-Ru-O-EO_x$  structure could be prepared. As such, we turned to the  $DPhF$  ( $DPhF = N,N'$ -diphenylformamidinate) and  $chp$  ( $chp = 6$ -chloro-2-hydroxypyridinate) ligands, for their steric bulk near the axial coordination site should eliminate the possibility of forming polymeric chains, and only one oxyanionic ligand should bind to the  $Ru_2$  core based on charge balance. The compounds discussed herein are given in [Chart 1](#).

**Chart 1. Compounds Discussed Herein**

Entry	Complex	Ligands
1	$Ru_2(DPhF)_4Cl$	 DPhF
2	$[Ru_2(DPhF)_4][NO_3]$	
3	$Ru_2(chp)_4Cl$	 chp
4	$Ru_2(chp)_4ONO_2$	
5	$Ru_2(chp)_4OClO_3$	

### Synthesis and IR Spectroscopic Characterization.

Compounds **2**, **4**, and **5** were prepared from the chloride precursors **1** and **3** by metathesis with the appropriate  $Ag^+$  salts ( $AgNO_3$  for **2** and **4**;  $AgClO_4$  for **5**) as shown in [Scheme 3](#). The IR spectrum for **2** displays a signal at  $1773\text{ cm}^{-1}$ , which is well within the characteristic range of  $1700\text{--}1800\text{ cm}^{-1}$  for free nitrate anions.<sup>19</sup> Furthermore, the MALDI-TOF mass spectrum of **2** shows an isotopic envelope indicative of the free  $[Ru_2(DPhF)_4]^+$  core ([Supporting Information, Figure S1](#)), and the crystal structure of **2** consists of well-separated  $[Ru_2(DPhF)_4]^+$  cations and  $NO_3^-$  anions.<sup>20</sup> The steric bulk of the  $DPhF$  phenyl rings therefore prevents  $NO_3^-$  coordination. In contrast, the IR spectra of **4** and **5** display signals consistent with O-coordinated nitrate<sup>19b</sup> and perchlorate ligands<sup>19b,21</sup> ( $1278\text{ cm}^{-1}$  [ $\nu_{\text{asym}}(\text{ONO})$ ] for **4**;  $\nu_4 = 1154, 1134, 1025\text{ cm}^{-1}$ , and  $\nu_2 = 894\text{ cm}^{-1}$  for **5**).

**Crystallography.** Compounds **4** and **5** have been characterized by X-ray crystallography ([Figures 1](#) and [2](#), and [Supporting Information, Table S1](#)). As with the chloride

**Scheme 3. Formation of Nitrate Complex 2 from Chloride Precursor 1 and Oxyanion Complexes 4 and 5 from Chloride Precursor 3**

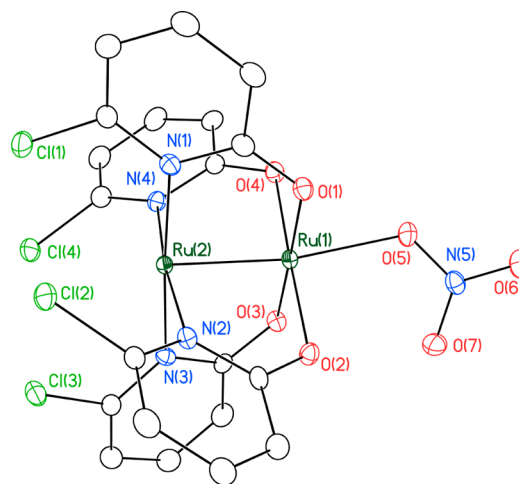
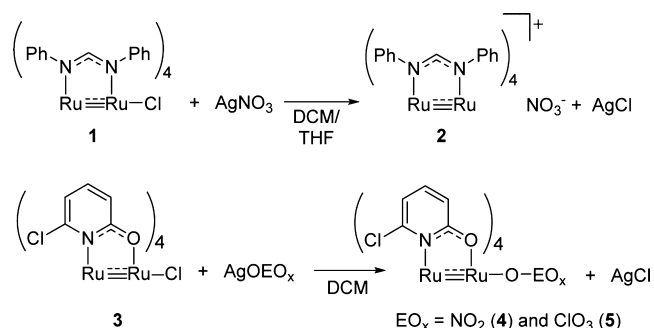


**Figure 1.** Thermal ellipsoid plot of  $4 \cdot 2CH_2Cl_2$  with ellipsoids drawn at the 50% probability level. Hydrogen atoms and molecules of solvation are omitted for clarity.

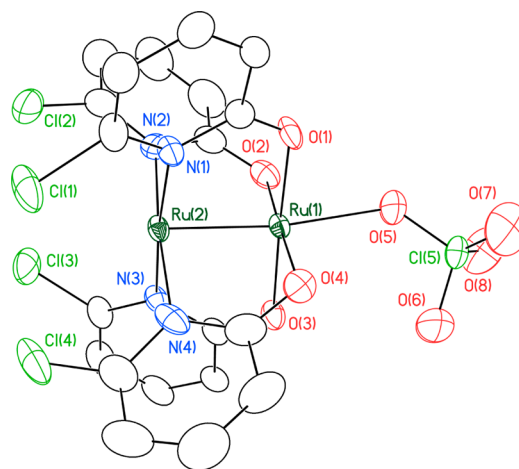


**Figure 2.** Thermal ellipsoid plot of  $5 \cdot 2CH_2Cl_2$  with ellipsoids drawn at the 50% probability level. Hydrogen atoms and molecules of solvation are omitted for clarity.

precursor **3**<sup>22</sup> and azide analogue  $Ru_2(chp)_4N_3$ ,<sup>2d</sup> the equatorial  $chp$  ligands in **4** and **5** are bound in a (4,0) orientation, which allows for the oxyanionic ligand to bind only to the exposed  $Ru$  axial site.

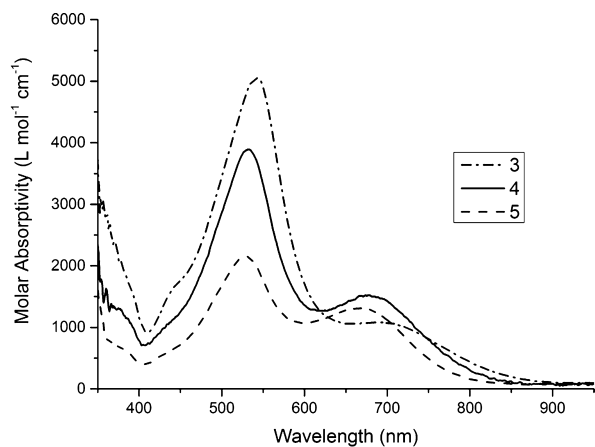
The  $Ru-Ru$  distances in **4** and **5** ( $2.2633(3)$  and  $2.2540(7)$  Å,<sup>23</sup> respectively, listed in [Table 1](#)) are in accord with all other

**Table 1.** Selected Crystallographic Bond Lengths and Angles for **4** and **5** (E = N for **4**, Cl for **5**)

	<b>4</b>	<b>5</b>
Ru(1)–Ru(2), Å	2.2633(3)	2.2540(7)
Ru(1)–O(5), Å	2.200(2)	2.249(4)
O(5)–E(5), Å	1.306(3)	1.464(4)
E(5)–O(6), Å	1.221(3)	1.445(6)
E(5)–O(7), Å	1.236(3)	1.370(5)
E(5)–O(8), Å	–	1.392(5)
Ru(2)–Ru(1)–O(5), °	170.07(6)	170.9(2)

previously characterized Ru<sub>2</sub><sup>5+</sup> oxypyridinate complexes.<sup>24</sup> The Ru(2)–Ru(1)–O(5) bond angle in **4** deviates from linearity to 170.07(7)°, and that in **5** deviates to 170.9(2)°, likely due to crystal packing effects. At 1.221(3) and 1.236(3) Å, the nitrate N–O distances (N(5)–O(6) and N(5)–O(7), respectively) in **4** are slightly shorter than, but in line with, those of an unbound nitrate anion (1.241(2) Å).<sup>25</sup> At 1.306(3) Å, the O(5)–N(5) distance is significantly longer, causing the nitrate anion to lose 3-fold symmetry due to the Ru(1)–O(5) interaction. The O(6)–N(5)–O(7) angle is 122.1(3)° and combining it with the other O–N–O angles (118.4(3)° and 119.4(2)°) sums to 359.9°, indicating a planar nitrate group, which is oriented parallel to the Ru–Ru bond. The perchlorate anion in **5** exhibits O–Cl–O angles that range from 107.0(3)° to 112.8(4)°, which are close to the idealized geometry of 109.5° for a tetrahedral anion. The O(5)–Cl(5) distance is slightly elongated, at 1.464(4) Å, compared to the other O–Cl bond distances of 1.370(5), 1.392(5), and 1.445(6) Å.

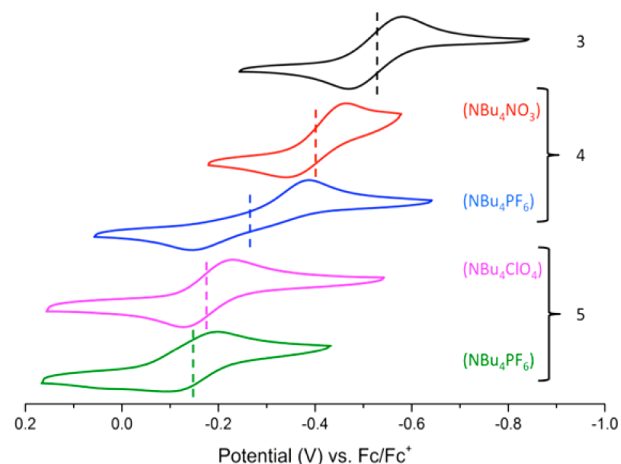
**UV/Vis Spectroscopy.** The most intense absorption feature for compounds **3–5** in CH<sub>2</sub>Cl<sub>2</sub> shifts from 529 to 532 to 542 nm and increases in intensity as the coordinating strength of the anion increases (**5** < **4** < **3**) (Figure 3). Though

**Figure 3.** UV/vis spectra for compounds **3–5** in CH<sub>2</sub>Cl<sub>2</sub>. The spectrum for **3** was previously reported<sup>22</sup> but is included here for direct comparison.

this electronic transition has not been definitively assigned, the variation in energy and intensity observed here suggests that it has significant LMCT character involving the axial ligand. The secondary feature in the spectrum also shifts from 666 to 678 to 689 nm in the same manner (**5** < **4** < **3**), but the intensity of this feature remains relatively consistent throughout the series.

**Cyclic Voltammetry.** Cyclic voltammograms of **4** and **5** were recorded under two distinct sets of conditions. Solutions of **3–5** in CH<sub>2</sub>Cl<sub>2</sub> with 0.1 M NBu<sub>4</sub>PF<sub>6</sub> electrolyte were

examined, as well as solutions of **4** with 0.1 M NBu<sub>4</sub>NO<sub>3</sub> and **5** with 0.1 M NBu<sub>4</sub>ClO<sub>4</sub>. These varying conditions give insight into the binding of NO<sub>3</sub><sup>−</sup> and ClO<sub>4</sub><sup>−</sup> anions to the [Ru<sub>2</sub>(chp)<sub>4</sub>]<sup>+</sup> core in solution. In analyzing these data we can consider two limiting cases. If, first, the NO<sub>3</sub><sup>−</sup> and ClO<sub>4</sub><sup>−</sup> anions dissociate completely from **4** and **5** in CH<sub>2</sub>Cl<sub>2</sub>, then we would expect both compounds to have identical CV traces in 0.1 M NBu<sub>4</sub>PF<sub>6</sub>. If, on the other hand, we assume that NO<sub>3</sub><sup>−</sup> and ClO<sub>4</sub><sup>−</sup> do not dissociate at all from **4** or **5** in solution, then we would expect the CV traces of **4** with NBu<sub>4</sub>PF<sub>6</sub> and NBu<sub>4</sub>NO<sub>3</sub> electrolytes to be identical, and the CV traces of **5** with NBu<sub>4</sub>PF<sub>6</sub> and NBu<sub>4</sub>ClO<sub>4</sub> to be identical as well. The data presented in Figure 4 (see also Table 2) show clearly that

**Figure 4.** Cyclic voltammograms of Ru<sub>2</sub><sup>5+/4+</sup> couple for **3–5** versus Fc/Fc<sup>+</sup>. E<sub>1/2</sub> for each species is marked with a dashed vertical line.**Table 2.** E values for Ru<sub>2</sub><sup>5+/4+</sup> Couple for **1–5** versus Fc/Fc<sup>+</sup> in CH<sub>2</sub>Cl<sub>2</sub> with Scan Rate = 100 mV/s and 0.1 M Electrolyte

compd	electrolyte	E <sub>1/2</sub> (V)	E <sub>c</sub> (V)	E <sub>a</sub> (V)
<b>1</b>	NBu <sub>4</sub> ClO <sub>4</sub>	–	−1.1 <sup>b</sup>	–
<b>2</b>	NBu <sub>4</sub> PF <sub>6</sub>	−0.687	–	–
<b>3</b>	NBu <sub>4</sub> PF <sub>6</sub>	−0.525 <sup>c</sup>	−0.581	−0.469
<b>4</b>	NBu <sub>4</sub> NO <sub>3</sub>	−0.401 <sup>a</sup>	−0.465	−0.338
<b>4</b>	NBu <sub>4</sub> PF <sub>6</sub>	−0.267 <sup>a</sup>	−0.388	−0.146
<b>5</b>	NBu <sub>4</sub> ClO <sub>4</sub>	−0.179 <sup>a</sup>	−0.230	−0.127
<b>5</b>	NBu <sub>4</sub> PF <sub>6</sub>	−0.145 <sup>a</sup>	−0.197	−0.094

<sup>a</sup>Indicates quasi-reversible. <sup>b</sup>Previously reported against SCE<sup>26b</sup> and converted here to be against Fc/Fc<sup>+</sup>.<sup>27</sup> <sup>c</sup>Previously reported against Ag/AgCl<sup>28</sup> and re-measured here for direct comparison.

neither of these limiting cases reflects reality. The fact that the CVs of **4** and **5** in NBu<sub>4</sub>PF<sub>6</sub> appear distinct indicates that these solutions do not simply contain free [Ru<sub>2</sub>(chp)<sub>4</sub>]<sup>+</sup> cations. However, the fact that the redox potentials change when the electrolyte is changed to NBu<sub>4</sub>NO<sub>3</sub> or NBu<sub>4</sub>ClO<sub>4</sub> indicates that both **4** and **5** undergo the following equilibrium in solution: Ru<sub>2</sub>(chp)<sub>4</sub>X ⇌ [Ru<sub>2</sub>(chp)<sub>4</sub>]<sup>+</sup> + X<sup>−</sup>. Other diruthenium compounds show similar behavior.<sup>26</sup> Addition of excess X<sup>−</sup> shifts this equilibrium to the left. This is clearly a fast equilibrium relative to the time scale of the electrochemical measurement since we do not observe distinct waves that may be assigned to Ru<sub>2</sub>(chp)<sub>4</sub>X and [Ru<sub>2</sub>(chp)<sub>4</sub>]<sup>+</sup>. These results indicate that both Ru<sub>2</sub>(chp)<sub>4</sub>X species and free X<sup>−</sup> are chemically relevant on the time scale of photolysis experiments in fluid solution at room temperature (vide infra).

**Photolysis Screening by Mass Spectrometry.** MALDI-TOF mass spectrometry is a particularly useful method for screening photolytically active compounds. In this case, the MALDI-TOF nitrogen laser (337 nm) is the light source, and photolysis products can be directly observed in the mass spectrum. The most prominent set of signals for **4** and **5** in MALDI-TOF mass spectrometry experiments corresponds to the  $\text{Ru}_2(\text{chp})_4^+$  core with the characteristic  $\text{Ru}_2$  isotopic distribution centered around  $m/z = 717$  amu, indicating facile loss of the axially bound oxyanions. In the case of **4**, there is a weak  $\text{Ru}_2$  signal centered at  $m/z = 733$  amu (Figure 5), which is

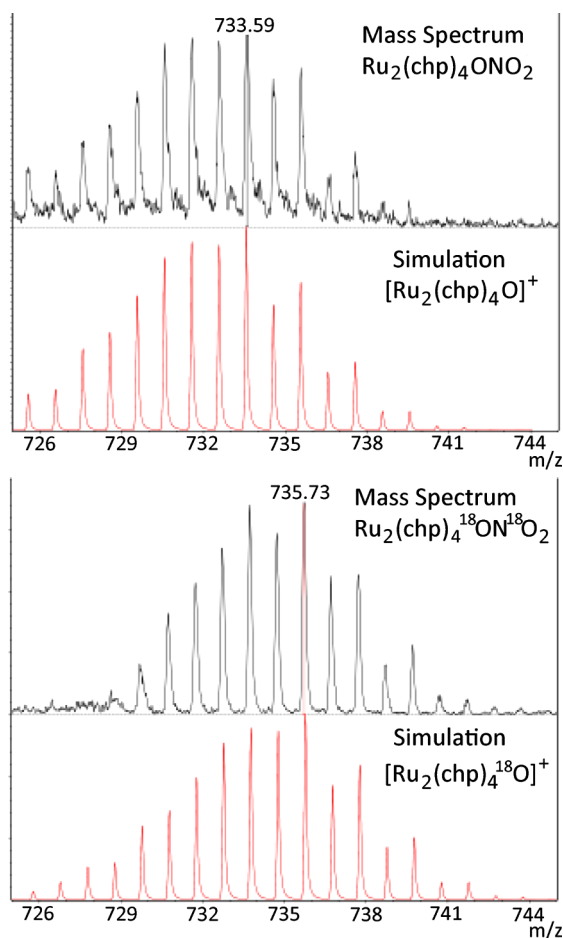


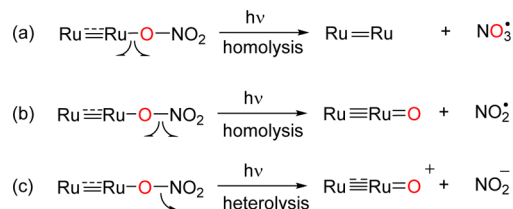
**Figure 5.** MALDI-TOF mass spectrum for **4** (black, top). Simulation (red) indicates isotope pattern at  $m/z = 733$  amu is due to  $[\text{Ru}_2(\text{chp})_4\text{O}]^+$ . Upon isotopic labeling, the MALDI-TOF mass spectrum for **4\*** (black, below) shifts by 2 units, as confirmed by simulation (red, bottom).

consistent with an  $[\text{Ru}_2(\text{chp})_4\text{O}]^+$  ion, suggesting that an  $\text{Ru}_2\text{O}$  species could be formed upon photolysis of **4**. This is also similar to the case of  $\text{Ru}_2$ -azide compounds that show  $\text{Ru}_2\text{N}$  signals in their mass spectra due to photolysis.<sup>2</sup> To further support this hypothesis, we used labeled  $^{18}\text{O}$ -nitrate ( $\text{N}^{18}\text{O}_3^-$ ) to form  $\text{Ru}_2(\text{chp})_4^{18}\text{ON}^{18}\text{O}_2$  (**4\***), and we found that the  $\text{Ru}_2\text{O}$  feature shifts in the mass spectrum to  $m/z = 735$  amu (Figure 5). This shift clearly indicates that the axial O atom in the  $[\text{Ru}_2(\text{chp})_4\text{O}]^+$  ion derives from nitrate and is fully consistent with photodissociation of  $\text{NO}_2^\bullet$  or  $\text{NO}_2^-$  from **4**. The  $m/z = 733$  amu feature is present but barely discernible in the spectrum of **5** (Figure S2), suggesting to us that perchlorate

may not be as suitable a precursor for the formation of an  $\text{Ru}_2\text{O}$  intermediate. Therefore, only **4** was investigated further.

In photolysis experiments of **4**, there are two possible sites at which bonds could break homolytically: (a) the  $\text{Ru}-\text{ONO}_2$  bond or (b) the  $\text{RuO}-\text{NO}_2$  bond (Scheme 4). Previous studies

#### Scheme 4. Possible Products upon Exposing Nitrate Complexes to Photolytic Conditions



have indicated that either site is possible.<sup>11a,b,29</sup> Heterolytic  $\text{RuO}-\text{NO}_2$  bond cleavage is another possible pathway (pathway c in Scheme 4), which has been demonstrated for perchlorate compounds.<sup>11b</sup> Both pathways b and c would explain our mass spectrometry results. Upon homolysis (pathway b), the resulting radical species  $\text{NO}_2^\bullet$  should be EPR active, unlike its  $\text{Ru}_2\text{O}$  counterpart,  $\text{Ru}_2(\text{chp})_4\text{O}$  (**6**), which is anticipated to have a ground state of  $S = 0$ .<sup>30</sup> Heterolysis (pathway c), on the other hand, would give rise to an EPR active  $\text{Ru}_2\text{O}^+$  species. Thus, we decided to use EPR spectroscopy to assess the mechanism of photolysis for **4**.

**Photolysis of 4 in Frozen Solution at 77 K and in Fluid Solution at Room Temperature.** The EPR spectra of **2**, **4**, and **5** (Figures S3, 6, and S4, respectively) were measured at 10

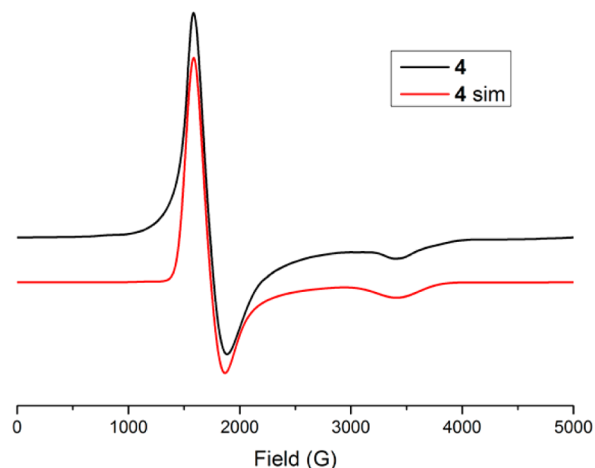


**Figure 6.** EPR spectrum and simulation of **4** recorded at 10 K.

or 15 K in a frozen solution of  $\text{CH}_2\text{Cl}_2$ . Though electrochemical measurements (vide supra) suggest the presence of an equilibrium between  $\text{Ru}_2$  bound and unbound nitrate species, the 10 K EPR spectrum of **4** can be modeled with a single axial signal with effective  $g$  values of 3.86 and 1.95, consistent with an  $S = 3/2$  ground state where  $D \gg h\nu$  (Table 3). Thus, the nitrate-bound **4** is most likely the dominant species in solution at this temperature, and its prominent EPR signal can be used to assess the efficacy of photolysis of **4** in frozen solution.

Exposure of a frozen  $\text{CH}_2\text{Cl}_2$  solution of **4** to 350 nm wavelength light at 77 K for 8 h yields no change in the intensity of the EPR signal of **4**. Switching to 254 nm light and

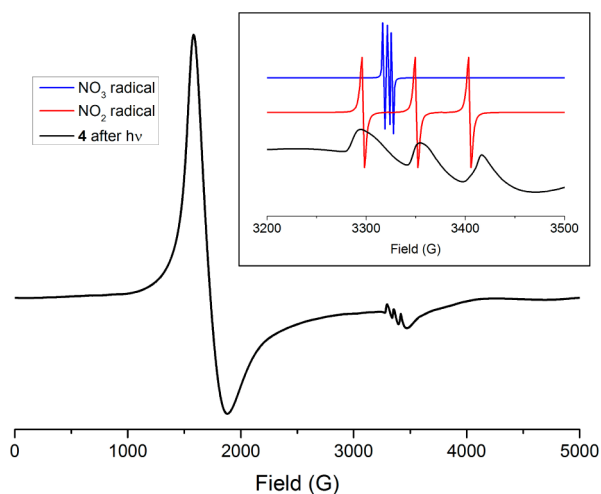


Table 3. EPR Spectral Simulations for 2, 4, and 5

	2	4	5
$g_{\perp}$	2.125	2.01	2.00
$g_{\parallel}$	1.94	1.95	1.93
$E/D$	0.006	0.035	0.033
HStrain <sup>a</sup>	850, 350, 450	1200, 900, 1200	1550, 850, 1100

<sup>a</sup>HStrain accounts for anisotropic line broadening due to unresolved hyperfine coupling.

photolyzing for 16 h at 77 K yields the EPR spectrum shown in Figure 7. There is a slight decrease in the signal intensity from



**Figure 7.** EPR spectrum of 4 in  $\text{CH}_2\text{Cl}_2$  taken at 10 K after 16 h of frozen photolysis using 254 nm light. Inset: Simulations<sup>31</sup> of  $\text{NO}_3^\bullet$  (blue, above) and  $\text{NO}_2^\bullet$  (red, middle) compared to 4 after frozen photolysis (black, below).

the  $S = 3/2$  signal of 4, and, more significantly, a new feature in the  $g = 2$  region is present. This new signal is an isotropic 1:1:1 triplet, clearly indicating a radical species with hyperfine coupling involving an  $I = 1$   $^{14}\text{N}$  nucleus, and it compares favorably to known literature values for  $\text{NO}_2^\bullet$  versus those of  $\text{NO}_3^\bullet$  (Figure 7, inset).<sup>31</sup> The presence of  $\text{NO}_2^\bullet$  suggests that, though photolysis of 4 proceeds in low yield at 77 K, homolytic cleavage of the O(S)–N(S) nitrate bond is the primary photolysis pathway (pathway b in Scheme 3).

In order to improve the yield of photolysis, subsequent experiments were performed on fluid solutions of 4 in  $\text{CH}_2\text{Cl}_2$  at room temperature under  $\text{N}_2$ . Under these conditions, photolysis is complete in a shorter time period of 4 h using 350 nm wavelength light. Using the isotopically enhanced analogue 4\*, GC-MS analysis of the headspace of the reaction confirms formation of  $\text{N}^{18}\text{O}_2^\bullet$  ( $m/z = 50$ ) in significant quantities (Figure 8), further supporting the homolytic cleavage mechanism (pathway b in Scheme 3) suggested by our EPR results.

**Oxygen Atom Transfer via Room-Temperature Photolysis of 4.** Room-temperature fluid solution photolytic experiments were also performed in the presence of an excess of the well-known oxygen atom acceptor  $\text{PPh}_3$  and monitored for the formation of oxygen atom transfer products. A  $\text{CH}_2\text{Cl}_2$  solution of 4 and  $\text{PPh}_3$  (20 equiv vs 4) was photolyzed for 4 h using 350 nm light at room temperature under  $\text{N}_2$ . Analysis by  $^{31}\text{P}\{^1\text{H}\}$  NMR spectroscopy indicates the formation of the intermolecular oxygen atom transfer product  $\text{OPPh}_3$  in >100%

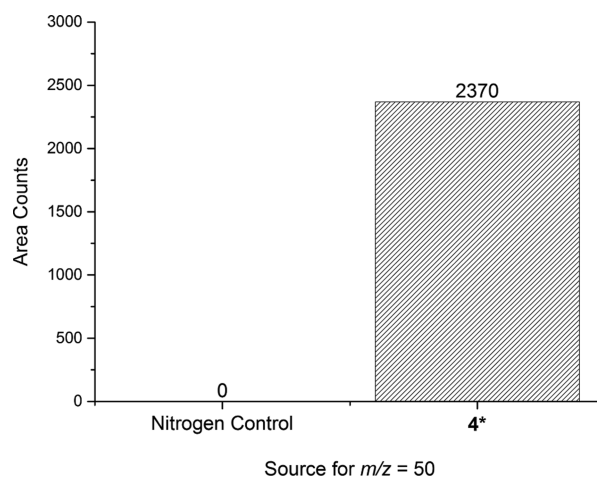


**Figure 8.** GC-MS headspace analysis for the formation of  $\text{N}^{18}\text{O}_2^\bullet$  ( $m/z = 50$ ) after photolysis of 4\* at room temperature under  $\text{N}_2$  for 4 h using 350 nm wavelength light. As compared to the counts for  $m/z = 50$  amu for the  $\text{N}_2$  control,  $\text{N}^{18}\text{O}_2^\bullet$  is clearly formed under the reaction conditions.

yield (determined by  $^{31}\text{P}$  NMR integration against a standard of  $\text{PPh}_4\text{Cl}$ ) (Figure 9). The identity of this product was confirmed

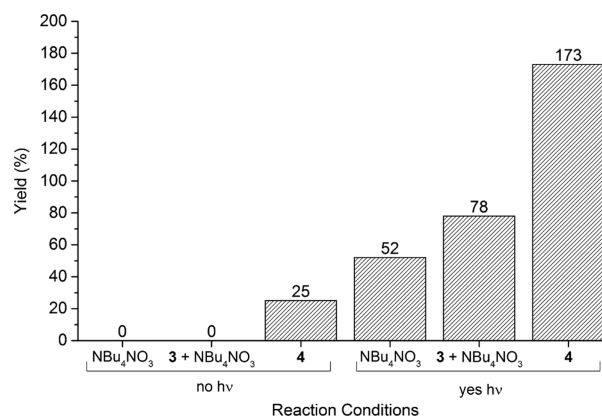


**Figure 9.** Yield of  $\text{OPPh}_3$  after exposure to different oxygen atom sources, both with and without exposure to photolytic conditions.

upon doping with an authentic sample of  $\text{OPPh}_3$  (Figure S5) and is further corroborated by ESI mass spectral data, which show that the product formed in this reaction with 4 has a mass of  $m/z = 279$  amu (consistent with  $\text{OPPh}_3$ ) (Figure S6) and shifts by 2 mass units to  $m/z = 281$  amu (consistent with  $^{18}\text{OPPh}_3$ ) upon using 4\* (Figure S7).

The >100% yield of  $\text{OPPh}_3$  implies that more than one active oxidant is formed under these conditions. As mentioned above, some amount of free  $\text{NO}_3^-$  is expected to be present based on our electrochemistry results. Upon UV irradiation at  $\sim 300$  nm, unbound nitrate is known to eliminate either  $^3\text{P O}$  or  $\text{O}^{-32}$  or to isomerize to peroxyxynitrite.<sup>33</sup> To test the possibility that unbound nitrate is the sole oxygen atom source, photolysis of  $\text{NBU}_4\text{NO}_3$  with  $\text{PPh}_3$  was performed under conditions identical to those previously expressed.  $\text{OPPh}_3$  is indeed generated but in less than one-third the yield as when 4 was used (Figure 9). We also considered the possibility that the  $\text{Ru}_2$  complex could simply act as a photosensitizer for free  $\text{NO}_3^-$ . A control reaction was therefore performed in which  $\text{NBU}_4\text{NO}_3$  and  $\text{PPh}_3$  were photolyzed in the presence of  $\text{Ru}_2(\text{chp})_4\text{Cl}$  (3) as a

photosensitizer (Figure 9).  $\text{OPPh}_3$  is generated in better yields here than without **3**, but this result still does not match our findings with **4**. Therefore,  $\text{OPPh}_3$  can be formed from free  $\text{NO}_3^-$  anion but is formed more efficiently from **4**.

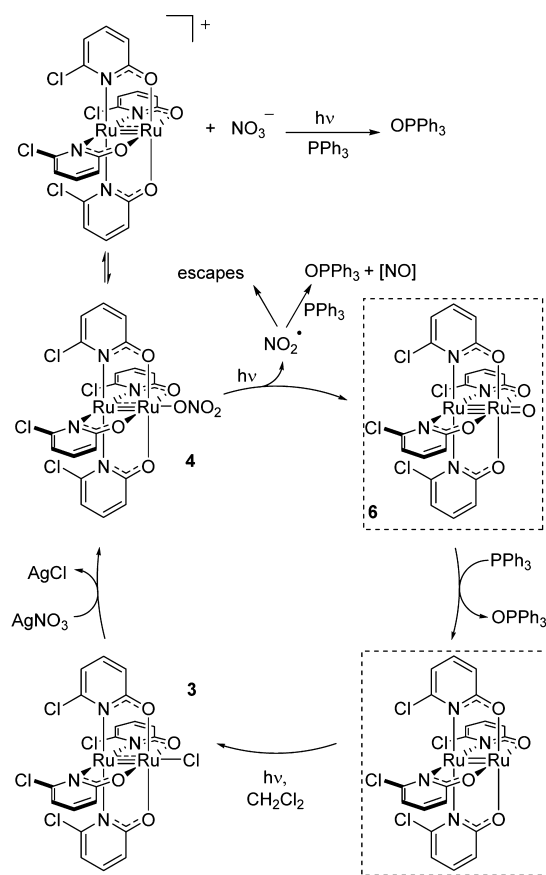
It is conceivable that  $\text{O}_2$  could be formed from either nitrate photolysis or bimetallic reductive coupling of  $\text{Ru}_2\text{O}$  intermediates and could be the oxygen atom source for formation of  $\text{OPPh}_3$ . To test this possibility, **4**\* was photolyzed in a  $\text{CH}_2\text{Cl}_2$  solution at room temperature and analysis of the reaction headspace was performed using GC-MS. These results indicate that  $^{18}\text{O}_2$  is not formed (Figure S8). Another potential oxygen atom source is the photolysis byproduct  $\text{NO}_2^\bullet$ .<sup>9b,10</sup> To probe this possibility,  $\text{PPh}_3$  was exposed to  $\text{NO}_2^\bullet$ . ESI mass spectral data indicate that the resulting product is indeed  $\text{OPPh}_3$  (Figure S9). To see whether  $\text{NO}_2^\bullet$  is fully consumed under our reaction conditions, **4** was photolyzed in a  $\text{CH}_2\text{Cl}_2$  solution containing 20 equiv of  $\text{PPh}_3$  at room temperature, and analysis of the reaction headspace was performed using GC-MS (Figure S10). Free  $\text{NO}_2^\bullet$  is still detected under these conditions, though in smaller yields than without  $\text{PPh}_3$  present. Thus,  $\text{NO}_2^\bullet$  is likely to be an oxygen atom source in this system but clearly cannot be the sole source. We therefore propose that the oxygen atom transfer in this system derives from three active oxidants: free  $\text{NO}_3^-$ ,  $\text{NO}_2^\bullet$ , and an  $\text{Ru}-\text{Ru}=\text{O}$  intermediate, giving yields of  $\text{OPPh}_3$  greater than 100%.

Finally, we were interested in determining the identity of the resulting  $\text{Ru}_2$  species after completion of room temperature photolysis in the presence of  $\text{PPh}_3$ . Only one  $\text{Ru}_2$  product was observed and isolated. MALDI-TOF mass spectrometry and UV/vis spectroscopy confirm this product to be the precursor **3**. This result was surprising to us since oxygen atom transfer from an  $\text{Ru}-\text{Ru}=\text{O}$  species should yield an  $\text{Ru}_2(\text{II}/\text{II})$  product such as  $\text{Ru}_2(\text{chp})_4\text{PPh}_3$ , a species that we have recently characterized.<sup>34</sup> However, low-valent metal–metal bonded dimers are known to react with light and halogenated solvents to yield one-electron-oxidized compounds bearing an axial halide ligand.<sup>35</sup> This reaction sequence explains the formation of **3** as shown in Scheme 5. Thus, our results present a complete synthetic photocycle for oxygen atom transfer from a photoactive oxyanion complex.

## CONCLUSIONS

Whereas the  $[\text{Ru}_2(\text{DPhF})_4]^+$  core is not sterically accessible to bind nonlinear anions as ligands, the  $[\text{Ru}_2(\text{chp})_4]^+$  core does support the formation of discrete, mono-oxyanion complexes with  $\eta^1$ -nitrate and -perchlorate anions. MALDI-TOF mass spectrometry, EPR, and GC-MS headspace analysis data suggest that photolysis of **4** proceeds to generate  $\text{Ru}-\text{Ru}=\text{O}$  species **6** and  $\text{NO}_2^\bullet$ . Room-temperature solution phase photolysis of **4** allows for oxygen atom transfer to  $\text{PPh}_3$  to form  $\text{OPPh}_3$  in a synthetic photocycle that regenerates **3**. We therefore propose that  $\text{PPh}_3$  is directly oxidized by a combination of three active oxidants: photosensitized free  $\text{NO}_3^-$ ,  $\text{NO}_2^\bullet$ , and the  $\text{Ru}_2\text{O}$  reactive intermediate **6**. This work demonstrates for the first time that the generation of a reactive metal oxo species from an oxyanion complex can be incorporated into a synthetic cycle. Further exploitation of these reaction conditions, along with efforts to stabilize and characterize the putative  $\text{Ru}-\text{Ru}=\text{O}$  intermediate, are underway in our laboratory.

## Scheme 5. Proposed Mechanistic Scheme for the Oxygen Atom Transfer Reaction Presented Here<sup>a</sup>



<sup>a</sup>Proposed intermediates **6** and  $\text{Ru}_2(\text{chp})_4$  are in dashed boxes.

## EXPERIMENTAL SECTION

**General Methods.** All syntheses were conducted under a dry  $\text{N}_2$  atmosphere using Schlenk line techniques unless otherwise noted; product workup and isolation were achieved in air unless otherwise noted. Dichloromethane ( $\text{CH}_2\text{Cl}_2$ ) was dried with  $\text{CaH}_2$  and distilled before use. Hexanes were obtained from a Vacuum Atmospheres Solvent System and degassed prior to use. All materials were commercially available and used as received, unless otherwise noted. Compounds **1**<sup>26b,36</sup> and **3**<sup>2d,22</sup> were prepared according to literature procedures. Photolysis of frozen samples of **4** was performed in a Rayonet RPR-200 photochemical reactor with light from 254 and 350 nm mercury vapor lamps.

**$[\text{Ru}_2(\text{DPhF})_4][\text{NO}_3]$  (**2**).**  $\text{Ru}_2(\text{DPhF})_4\text{Cl}$  (200 mg, 0.196 mmol, 1 equiv) was dissolved in  $\text{CH}_2\text{Cl}_2$  and added to a suspension of  $\text{AgNO}_3$  (500 mg, 2.94 mmol, 15 equiv) in 3 mL of THF in air. The mixture changed color from green to purple-blue almost instantaneously and was allowed to continue stirring at room temperature (RT) overnight. The solids were filtered off, and the remaining solution was left to evaporate slowly to yield dark purple crystals of the product. Yield: 180 mg, 87.7%. MW: 1045.10  $\text{g mol}^{-1}$ . MALDI-TOF ( $m/z$ ): ( $[\text{M} - \text{NO}_3]^+$ ) 984. IR (ATR): 3053, 1773 [ $\nu_{\text{sym}} \text{NO}_3$ ], 1591, 1520, 1486, 1449, 1364, 1349, 1314, 1214, 1175, 1156, 1078, 1027, 936, 827, 761, 693, 668, 658, 619  $\text{cm}^{-1}$ . UV/vis ( $\text{CH}_2\text{Cl}_2$ ):  $\lambda_{\text{max}}$  ( $\epsilon$ ) = 437 (4250), 527 (5950), 681 (7170  $\text{mol}^{-1} \text{L cm}^{-1}$ ). [ $\text{C}_{52}\text{H}_{44}\text{N}_9\text{O}_3\text{Ru}_2 \cdot \text{CH}_2\text{Cl}_2 \cdot 2\text{H}_2\text{O}$ ]: calcd C 54.59, H 4.32, N 10.81; found C 54.31, H 3.88, N 11.37. Crystals suitable for X-ray diffraction were grown via slow evaporation from a concentrated solution of  $\text{CH}_2\text{Cl}_2$  at RT.

**$\text{Ru}_2(\text{chp})_4\text{ONO}_2$  (**4**).**  $\text{Ru}_2(\text{chp})_4\text{Cl}$  (200.0 mg, 0.266 mmol, 1 equiv) and  $\text{AgNO}_3$  (54.6 mg, 0.321 mmol, 1.2 equiv) were dissolved in 30 mL of freshly distilled  $\text{CH}_2\text{Cl}_2$  and allowed to stir for 96 h at RT under  $\text{N}_2$ . A white precipitate ( $\text{AgCl}$ ) formed. The reaction mixture was filtered

through a fine sintered glass frit. Excess  $\text{CH}_2\text{Cl}_2$  was washed through the frit until it was no longer colored. The filtrate was removed under reduced pressure, and the resulting purple solid was washed with hexanes and collected. Yield: 195.5 mg, 94.4%. MW: 778.29  $\text{g mol}^{-1}$ . MALDI-TOF ( $m/z$ ):  $([\text{M} - \text{NO}_2]^+)$  733,  $([\text{M} - \text{ONO}_2]^+)$  717. IR (ATR): 3108, 2964, 1596, 1534, 1465, 1434, 1390, 1350, 1278 [ $\nu_{\text{asym}}(\text{ONO})$ ], 1262, 1181, 1085, 1011, 964, 942, 931, 866, 795, 789, 724, 630  $\text{cm}^{-1}$ . UV/vis ( $\text{CH}_2\text{Cl}_2$ ):  $\lambda_{\text{max}}(\epsilon) = 532$  (3890), 678 (1520  $\text{mol}^{-1} \text{L cm}^{-1}$ ).  $[\text{C}_{20}\text{H}_{12}\text{Cl}_4\text{N}_3\text{O}_7\text{Ru}_2]$ : calcd C 30.86, H 1.55, N 8.99; found C 30.64, H 1.44, N 8.81. Crystals suitable for X-ray diffraction were grown from a saturated  $\text{CH}_2\text{Cl}_2$  solution at  $-80^\circ\text{C}$ .

$\text{Ru}_2(\text{chp})_4\text{OCIO}_3$  (**5**).  $\text{Ru}_2(\text{chp})_4\text{Cl}$  (200.0 mg, 0.266 mmol, 1 equiv) and  $\text{AgClO}_4$  (66.7 mg, 0.322 mmol, 1.2 equiv) were dissolved in 30 mL of freshly distilled  $\text{CH}_2\text{Cl}_2$  and allowed to stir for 96 h at RT under  $\text{N}_2$ . A white precipitate ( $\text{AgCl}$ ) formed. The reaction mixture was filtered through a fine sintered glass frit. Excess  $\text{CH}_2\text{Cl}_2$  was washed through the frit until it was no longer colored. The filtrate was concentrated under reduced pressure, and the resulting purple solid was washed with hexanes and collected. Yield: 205.3 mg, 94.6%. MW: 815.74  $\text{g mol}^{-1}$ . MALDI-TOF ( $m/z$ ):  $([\text{M} - \text{ClO}_3]^+)$  733,  $([\text{M} - \text{OCIO}_3]^+)$  717. IR (ATR): 3107, 1596, 1536, 1433, 1391, 1337, 1263, 1154 [ $\nu_4$ ], 1134 [ $\nu_4$ ], 1075, 1025 [ $\nu_4$ ], 1013, 932, 894 [ $\nu_2$ ], 790, 723, 705, 668, 632, 610  $\text{cm}^{-1}$ . UV/vis ( $\text{CH}_2\text{Cl}_2$ ):  $\lambda_{\text{max}}(\epsilon) = 529$  (2150), 666 (1310  $\text{mol}^{-1} \text{L cm}^{-1}$ ).  $[\text{C}_{20}\text{H}_{12}\text{Cl}_5\text{N}_4\text{O}_8\text{Ru}_2]$ : calcd C 29.45, H 1.48, N 6.87; found C 29.20, H 1.68, N 6.26. Crystals suitable for X-ray diffraction were grown from a saturated  $\text{CH}_2\text{Cl}_2$  solution layered with hexanes at RT. **Caution!** Anhydrous metal perchlorate complexes are potentially explosive.

$\text{AgN}^{18}\text{O}_3$ . First, 0.1 g of  $\text{HN}^{18}\text{O}_3$  (95 atom %, 65 wt % in  $\text{H}_2^{18}\text{O}$ ), 0.1 g of  $\text{H}_2^{18}\text{O}$ , Ag powder, and a stir bar were added to a vial that was subsequently capped. This heterogeneous mixture was stirred at  $50^\circ\text{C}$  in air for 48 h; periodically the mixture was manually rotated and the solvent mixture forced to the bottom of the vial as it had crept up the walls of the vial. A white solid became visible as the reaction reached completion, which was re-dissolved in the  $\text{H}_2^{18}\text{O}$ . The supernatant liquid was then decanted away (using a pipet) from the heterogeneous solid mixture into a new vial and allowed to evaporate to dryness, leaving a crystalline product, which was dried under vacuum at  $50^\circ\text{C}$  overnight. Yield: 126.8 mg (76.5%). IR (ATR): 1676, 1657 [ $\nu_{\text{asym}}(^{18}\text{ON}^{18}\text{O})$ ], 1293 [ $\nu_{\text{sym}}(^{18}\text{ON}^{18}\text{O})$ ], 792 [ $\nu(^{18}\text{N}^{18}\text{O})$ ], 694  $\text{cm}^{-1}$ .

$\text{Ru}_2(\text{chp})_4^{18}\text{ON}^{18}\text{O}_2$  (**4\***).  $\text{AgN}^{18}\text{O}_3$  was ground into fine powder and then used in a procedure identical to that described for **4**. Yield: 141.2 mg, 67.7%. MW: 784.29  $\text{g mol}^{-1}$ . MALDI-TOF ( $m/z$ ):  $([\text{M} - \text{N}^{18}\text{O}_2]^+)$  735. IR (ATR): 3108, 2964, 1596, 1534, 1465, 1434, 1390, 1350, 1253 [ $\nu_{\text{asym}}(^{18}\text{ON}^{18}\text{O})$ ], 1262, 1181, 1085, 1011, 942, 931, 866, 795, 789, 724, 630  $\text{cm}^{-1}$ .

**Solution-Phase Reactions.** A 0.5 mM  $\text{CH}_2\text{Cl}_2$  solution of the nitrate source (**4**, **3** +  $\text{NBu}_4\text{NO}_3$ , or  $\text{NBu}_4\text{NO}_3$ ) with a 20-fold excess of  $\text{PPh}_3$  was prepared on a 30 mL scale in a quartz Schlenk tube (flask "A"). A 10 mL aliquot was transferred to a different flask (flask "B"), which was wrapped in foil, and allowed to stir under  $\text{N}_2$  for 4 h without exposure to photolytic conditions. The remaining 20 mL of solution was photolyzed in flask "A" under static vacuum at RT using 350 nm light for 4 h. After that time, a 10 mL aliquot was removed and transferred to a 25 mL Schlenk flask (flask "C"). Solutions in flasks "B" and "C" were reduced to dryness under vacuum and analyzed by NMR spectroscopy with a known quantity (1 equiv based on **4**) of  $\text{PPh}_4\text{Cl}$  added for use as a comparative standard.  $^{31}\text{P}\{^1\text{H}\}$  NMR (298 K, 400 MHz,  $\text{CDCl}_3$ ):  $\delta$  29 (OPPh<sub>3</sub>), 23 (PPh<sub>4</sub>Cl),  $-5.5$  (PPh<sub>3</sub>).

**Physical Measurements.** Matrix-assisted laser desorption/ionization time-of-flight (MALDI-TOF) mass spectrometry data were obtained using an anthracene matrix on a Bruker ULTRAFLEX III mass spectrometer equipped with a SmartBeam laser in positive ion detection mode. Electrospray ionization (ESI) mass spectrometry data were collected on a Thermo Q Exactive Plus mass spectrometer, and gas chromatography–mass spectrometry (GC-MS) data were collected on a Shimadzu GCMS-QP2010 Ultra spectrometer.  $^1\text{H}$  and  $^{31}\text{P}\{^1\text{H}\}$  data were obtained using a Bruker Avance III 400 MHz spectrometer. UV/vis spectra were obtained using a StellarNet Miniature BLUE-wave UV/vis dip probe with a tungsten–krypton

light source and a 10 mm path length tip. Infrared (IR) spectra were taken on a Bruker Tensor 27 spectrometer using an ATR adapter (no matrix). Cyclic voltammograms (CVs) were taken on a BASi Potentiostat using Epsilon software in  $\text{CH}_2\text{Cl}_2$  solutions with 0.1 M electrolyte and 1.0 mM substrate. The electrodes were as follows: glassy carbon (working), Pt wire (auxiliary), and  $\text{Ag}/\text{Ag}^+$  in  $\text{CH}_3\text{CN}$  (reference). The potentials were referenced versus the ferrocene/ferrocenium redox couple by externally added ferrocene. Elemental analysis was performed by Midwest Microlab, LLC, Indianapolis, IN, USA.

**EPR Spectroscopy.** EPR data were acquired on a Bruker ELEXSYS E500 EPR spectrometer equipped with a Varian E102 microwave bridge interfaced with a Linux system. An Oxford Instruments ESR-900 continuous-flow helium flow cryostat and an Oxford Instruments 3120 temperature controller were used to control the sample temperature. A Hewlett-Packard 432A power meter was used for microwave power calibration, with measurement conditions as follows: for **2**, 9.3762 GHz, 4 G modulation amplitude, 2500 G center field, 5000 G sweep width, 5.024 mW power, 55 dB gain, 327.68 ms time constant, 10 ms conversion time, and 15 K; for **4**, 9.3765 GHz, 4 G modulation amplitude, 2500 G center field, 5000 G sweep width, 5.024 mW power, 60 dB gain, 655.36 ms time constant, 10 ms conversion time, and 10 K; for **4-hv/NO<sub>2</sub><sup>\*</sup>**, 9.3765 GHz, 4 G modulation amplitude, 2500 G center field, 5000 G sweep width, 5.024 mW power, 60 dB gain, 655.36 ms time constant, 10 ms conversion time, and 10 K; for **5**, 9.3832 GHz, 4 G modulation amplitude, 2500 G center field, 5000 G sweep width, 5.024 mW power, 55 dB gain, 655.36 ms time constant, 10 ms conversion time, and 10 K. Spectral simulations were performed using the program EasySpin.<sup>37</sup>

**X-ray Crystallographic Data Collection and Structure Determination.** Crystallographic data were measured at the Molecular Structure Laboratory of the Chemistry Department of the University of Wisconsin–Madison. Suitable crystals of **4** and **5** were selected under oil and ambient conditions. For **4**, a purple block-shaped crystal with dimensions  $0.728 \times 0.374 \times 0.216 \text{ mm}^3$  was selected, and for **5** a purple plate crystal with dimensions  $0.166 \times 0.155 \times 0.094 \text{ mm}^3$  was chosen. The crystals were attached to the tip of a MiTeGen MicroMount tool, mounted in a stream of cold nitrogen at 100(1) K, and centered in the X-ray beam using a video monitoring system. The crystal evaluation and data collection were performed on a Bruker Quazar SMART APEX-II diffractometer with  $\text{Mo K}\alpha$  ( $\lambda = 0.71073 \text{ \AA}$ ) radiation. The data were collected using a routine to survey the reciprocal space to the extent of a full sphere to a resolution of 0.70  $\text{\AA}$  for **4** and 0.80  $\text{\AA}$  for **5** and were indexed by the APEX program.<sup>38</sup> The structures were solved via direct methods and refined by iterative cycles of least-squares refinement on  $F^2$  followed by difference Fourier synthesis. All hydrogen atoms were included in the final structure factor calculation at idealized positions and were allowed to ride on the neighboring atoms with relative isotropic displacement coefficients. Absorption corrections were based on a fitted function to the empirical transmission surface as sampled by multiple equivalent measurements.<sup>39</sup> The systematic absences in the diffraction data were uniquely consistent with the space groups  $P2_1/c$  for **4** and  $P2_1/n$  for **5**, yielding chemically reasonable and computationally stable results of refinement, and both structures were solved using direct methods using XS software.<sup>40</sup> Compound **4** is a pseudo-merohedral twin with a twin component ratio of 54:46. The twin components are related by a  $180^\circ$  rotation about  $[1\ 0\ 0]$ . Compound **5** is a non-merohedral twin with a twin component ratio of 60:40. The twin components are related by a  $180^\circ$  rotation about  $[0\ 0\ 1]$ .

## ■ ASSOCIATED CONTENT

### 📄 Supporting Information

The Supporting Information is available free of charge on the ACS Publications website at DOI: 10.1021/jacs.6b05942.

MALDI-MS and EPR spectra and simulations for **2** and **5**; crystallographic data for **4** and **5**, including tables for



selected bond distances and angles;  $^{31}\text{P}\{^1\text{H}\}$  NMR and ESI data for formation of  $(^{18})\text{OPPh}_3$  (PDF)  
X-ray crystallographic data for **4** and **5** (CIF)

## AUTHOR INFORMATION

### Corresponding Author

\*berry@chem.wisc.edu

### Present Address

<sup>‡</sup>J.S.P.: MTA Centre for Energy Research, Surface Chemistry, and Catalysis Department, P.O. Box 49, H-1525 Budapest, Hungary.

### Notes

The authors declare no competing financial interest.

## ACKNOWLEDGMENTS

We thank the U.S. Department of Energy, Chemical Sciences, Geosciences, and Biosciences Division, Office of Basic Energy Sciences, Office of Science (DE-FG02-10ER16204). A.R.C. thanks the National Science Foundation for a Graduate Research Fellowship (DGE-0718123). NMR and EPR facilities at UW-Madison are supported by the NSF (CHE-1048642 and CHE-0741901, respectively), and mass spectrometry instruments are funded by NIH (1S10 OD020022-1 and NCRR 1S10RR024601-01). We thank Dr. Ilia Guzei for crystallographic insights and Dr. Linghong Zhang for assistance with GC-MS measurements.

## REFERENCES

- (1) (a) Yoon, T. P.; Ischay, M. A.; Du, J. *Nat. Chem.* **2010**, *2*, 527. (b) Prier, C. K.; Rankic, D. A.; MacMillan, D. W. C. *Chem. Rev.* **2013**, *113*, 5322.
- (2) (a) Pap, J. S.; DeBeer George, S.; Berry, J. F. *Angew. Chem., Int. Ed.* **2008**, *47*, 10102. (b) Musch Long, A. K.; Yu, R. P.; Timmer, G. H.; Berry, J. F. *J. Am. Chem. Soc.* **2010**, *132*, 12228. (c) Long, A. K. M.; Timmer, G. H.; Pap, J. S.; Snyder, J. L.; Yu, R. P.; Berry, J. F. *J. Am. Chem. Soc.* **2011**, *133*, 13138. (d) Corcos, A. R.; Long, A. K. M.; Guzei, I. A.; Berry, J. F. *Eur. J. Inorg. Chem.* **2013**, *2013*, 3808.
- (3) (a) Schlangen, M.; Neugebauer, J.; Reiher, M.; Schröder, D.; López, J. P.; Haryono, M.; Heinemann, F. W.; Grohmann, A.; Schwarz, H. *J. Am. Chem. Soc.* **2008**, *130*, 4285. (b) Izzet, G.; Ishow, E.; Delaire, J.; Afonso, C.; Tabet, J. C.; Proust, A. *Inorg. Chem.* **2009**, *48*, 11865. (c) Scepaniak, J. J.; Young, J. A.; Bontchev, R. P.; Smith, J. M. *Angew. Chem., Int. Ed.* **2009**, *48*, 3158. (d) Schöffel, J.; Rogachev, A. Y.; DeBeer George, S.; Burger, P. *Angew. Chem., Int. Ed.* **2009**, *48*, 4734. (e) Hojilla Atienza, C. C.; Bowman, A. C.; Lobkovsky, E.; Chirik, P. J. *J. Am. Chem. Soc.* **2010**, *132*, 16343. (f) Thomson, R. K.; Cantat, T.; Scott, B. L.; Morris, D. E.; Batista, E. R.; Kiplinger, J. L. *Nat. Chem.* **2010**, *2*, 723. (g) Scheibel, M. G.; Askevold, B.; Heinemann, F. W.; Reijerse, E. J.; de Bruin, B.; Schneider, S. *Nat. Chem.* **2012**, *4*, 552. (h) Scheibel, M. G.; Wu, Y.; Stückl, A. C.; Krause, L.; Carl, E.; Stalke, D.; de Bruin, B.; Schneider, S. *J. Am. Chem. Soc.* **2013**, *135*, 17719. (i) Torres-Alacan, J.; Das, U.; Filippou, A. C.; Vöhringer, P. *Angew. Chem., Int. Ed.* **2013**, *52*, 12833. (j) Zolnhofer, E. M.; Käß, M.; Khusniyarov, M. M.; Heinemann, F. W.; Maron, L.; van Gastel, M.; Bill, E.; Meyer, K. *J. Am. Chem. Soc.* **2014**, *136*, 15072. (k) Sieh, D.; Burger, P. *Z. Anorg. Allg. Chem.* **2015**, *641*, 52. (l) Vreeken, V.; Siegler, M. A.; de Bruin, B.; Reek, J. N. H.; Lutz, M.; van der Plug, J. I. *Angew. Chem., Int. Ed.* **2015**, *54*, 7055. (m) Abbenseth, J.; Finger, M.; Wurtele, C.; Kasanmascheff, M.; Schneider, S. *Inorg. Chem. Front.* **2016**, *3*, 469. (n) Camp, C.; Grant, L. N.; Bergman, R. G.; Arnold, J. *Chem. Commun.* **2016**, *52*, 5538.
- (4) (a) Smith, J. M. *Prog. Inorg. Chem.* **2014**, *58*, 417. (b) Berry, J. F. *Comments Inorg. Chem.* **2009**, *30*, 28.
- (5) (a) Nugent, W. A.; Mayer, J. M. *Metal-Ligand Multiple Bonds*; John Wiley & Sons: New York, 1988. (b) Yin, G. *Coord. Chem. Rev.*

- 2010**, *254*, 1826. (c) Winkler, J. R.; Gray, H. B. In *Molecular Electronic Structures of Transition Metal Complexes I*; Mingos, D. M. P., Day, P., Dahl, J. P., Eds.; Springer: Berlin/Heidelberg, 2012; Vol. 142, p 17. (d) Ray, K.; Heims, F.; Pfaff, F. F. *Eur. J. Inorg. Chem.* **2013**, *2013*, 3784. (e) Chen, Z.; Yin, G. *Chem. Soc. Rev.* **2015**, *44*, 1083. (f) Ray, K.; Heims, F.; Schwalbe, M.; Nam, W. *Curr. Opin. Chem. Biol.* **2015**, *25*, 159.
- (6) (a) Moyer, B. A.; Meyer, T. J. *J. Am. Chem. Soc.* **1978**, *100*, 3601. (b) Moyer, B. A.; Meyer, T. J. *Inorg. Chem.* **1981**, *20*, 436. (c) Che, C.-M.; Wong, K.-Y.; Mak, T. C. W. *J. Chem. Soc., Chem. Commun.* **1985**, *0*, 546. (d) Che, C.-M.; Wong, K.-Y.; Mak, T. C. W. *J. Chem. Soc., Chem. Commun.* **1985**, 988. (e) Che, C. M.; Lai, T. F.; Wong, K. Y. *Inorg. Chem.* **1987**, *26*, 2289. (f) Che, C.-M.; Tang, W.-T.; Lee, W.-O.; Wong, W.-T.; Lai, T.-F. *J. Chem. Soc., Dalton Trans.* **1989**, 2011. (g) Che, C. M.; Tang, W. T.; Wong, W. T.; Lai, T. F. *J. Am. Chem. Soc.* **1989**, *111*, 9048. (h) Dengel, A. C.; Griffith, W. P.; O'Mahoney, C. A.; Williams, D. J. *J. Chem. Soc., Chem. Commun.* **1989**, 1720. (i) Nagao, H.; Nishimura, H.; Kitanaka, Y.; Howell, F. S.; Mukaida, M.; Kakihana, H. *Inorg. Chem.* **1990**, *29*, 1693. (j) Power, J. M.; Evertz, K.; Henling, L.; Marsh, R.; Schaefer, W. P.; Labinger, J. A.; Bercaw, J. E. *Inorg. Chem.* **1990**, *29*, 5058. (k) de Souza, V. R.; Nunes, G. S.; Rocha, R. C.; Toma, H. E. *Inorg. Chim. Acta* **2003**, *348*, 50. (l) Huynh, M. H. V.; Meyer, T. J. *Chem. Rev.* **2007**, *107*, 5004. (m) Gagliardi, C. J.; Westlake, B. C.; Kent, C. A.; Paul, J. J.; Papanikolas, J. M.; Meyer, T. J. *Coord. Chem. Rev.* **2010**, *254*, 2459. (n) Warren, J. J.; Tronic, T. A.; Mayer, J. M. *Chem. Rev.* **2010**, *110*, 6961.
- (7) Man, W.-L.; Lam, W. W. Y.; Wong, W.-Y.; Lau, T.-C. *J. Am. Chem. Soc.* **2006**, *128*, 14669.
- (8) Wong, K.-Y.; Che, C.-M.; Yip, W.-H.; Wang, R.-J.; Mak, T. C. W. *J. Chem. Soc., Dalton Trans.* **1992**, 1417.
- (9) (a) Suslick, K. S.; Acholla, F. V.; Cook, B. R. *J. Am. Chem. Soc.* **1987**, *109*, 2818. (b) Suslick, K. S.; Watson, R. A. *Inorg. Chem.* **1991**, *30*, 912.
- (10) Kunkely, H.; Vogler, A. *J. Am. Chem. Soc.* **1995**, *117*, 540.
- (11) (a) Harischandra, D. N.; Zhang, R.; Newcomb, M. *J. Am. Chem. Soc.* **2005**, *127*, 13776. (b) Zhang, R.; Newcomb, M. *Acc. Chem. Res.* **2008**, *41*, 468. (c) Zhang, R.; Vanover, E.; Luo, W.; Newcomb, M. *Dalton Trans.* **2014**, *43*, 8749.
- (12) Cheng, M.; Bakac, A. *J. Am. Chem. Soc.* **2008**, *130*, 5600.
- (13) (a) Nippe, M.; Goodman, S. M.; Fry, C. G.; Berry, J. F. *J. Am. Chem. Soc.* **2011**, *133*, 2856. (b) Brogden, D. W.; Turov, Y.; Nippe, M.; Li Manni, G.; Hillard, E. A.; Clérac, R.; Gagliardi, L.; Berry, J. F. *Inorg. Chem.* **2014**, *53*, 4777. (c) Brogden, D. W.; Berry, J. F. *Chem. Commun.* **2015**, *51*, 9153.
- (14) Villalobos, L.; Barker Paredes, J. E.; Cao, Z.; Ren, T. *Inorg. Chem.* **2013**, *52*, 12545.
- (15) Goberna-Ferrón, S.; Peña, B.; Soriano-López, J.; Carbó, J. J.; Zhao, H.; Poblet, J. M.; Dunbar, K. R.; Galán-Mascarós, J. R. *J. Catal.* **2014**, *315*, 25.
- (16) Ring, S.; Meijer, A. J. H. M.; Patmore, N. J. *Polyhedron* **2016**, *103*, 87.
- (17) Xu, G.-L.; Jablonski, C. G.; Ren, T. *Inorg. Chim. Acta* **2003**, *343*, 387.
- (18) Dunlop, K.; Wang, R.; Stanley Cameron, T.; Aquino, M. A. S. *J. Mol. Struct.* **2014**, *1058*, 122.
- (19) (a) Lever, A. B. P.; Mantovani, E.; Ramaswamy, B. S. *Can. J. Chem.* **1971**, *49*, 1957. (b) Nakamoto, K. *Infrared and Raman Spectra of Inorganic and Coordination Compounds. Part B: Applications in Coordination, Organometallic, and Bioinorganic Chemistry*, 5th ed.; John Wiley & Sons: New York, 1997.
- (20) Crystallographic data for  $[\text{Ru}_2(\text{DPhF})_4](\text{NO}_3)$ : space group =  $C2/c$ ; unit cell dimensions  $a = 14.028 \text{ \AA}$ ;  $b = 13.571 \text{ \AA}$ ;  $c = 23.189 \text{ \AA}$ ;  $\beta = 91.33^\circ$ ;  $V = 4413.60 \text{ \AA}^3$ .
- (21) Gowda, N. M. N.; Naikar, S. B.; Reddy, G. K. N. In *Advances in Inorganic Chemistry*; Emeleus, H. J., Sharpe, A. G., Eds.; Academic Press: 1984; Vol. Vol. 28, p 255.
- (22) Chakravarty, A. R.; Cotton, F. A.; Tocher, D. A. *Inorg. Chem.* **1985**, *24*, 1263.



(23) Bond distances and angles for minor component (8.82%) of another Ru(1) atom not reported here.

(24) Based on a search of the Cambridge Structural Database.

(25) Cherin, P.; Hamilton, W. C.; Post, B. *Acta Crystallogr.* **1967**, *23*, 455.

(26) (a) Lin, C.; Ren, T.; Valente, E. J.; Zubkowski, J. D.; Smith, E. T. *Chem. Lett.* **1997**, *26*, 753. (b) Bear, J. L.; Han, B.; Huang, S.; Kadish, K. M. *Inorg. Chem.* **1996**, *35*, 3012. (c) Kadish, K. M.; Garcia, R.; Phan, T.; Wellhoff, J.; Van Caemelbecke, E.; Bear, J. L. *Inorg. Chem.* **2008**, *47*, 11423. (d) Pap, J. S.; Snyder, J. L.; Piccoli, P. M. B.; Berry, J. F. *Inorg. Chem.* **2009**, *48*, 9846.

(27) Connelly, N. G.; Geiger, W. E. *Chem. Rev.* **1996**, *96*, 877.

(28) Chakravarty, A. R.; Cotton, F. A.; Tocher, D. A.; Tocher, J. H. *Polyhedron* **1985**, *4*, 1475.

(29) (a) Berry, J. F.; Bill, E.; Bothe, E.; George, S. D.; Mienert, B.; Neese, F.; Wieghardt, K. *Science* **2006**, *312*, 1937. (b) Chen, T.-H.; Asiri, N.; Kwong, K. W.; Malone, J.; Zhang, R. *Chem. Commun.* **2015**, *51*, 9949.

(30) (a) The corresponding Ru—Ru≡N complex has been shown unambiguously to have an  $S = 1/2$  ground state with an unpaired electron in the Ru—Ru  $\delta^*$  orbital.<sup>2</sup> The addition of one more electron upon changing N to O is therefore expected to fill the  $\delta^*$  level yielding a diamagnetic ground state. (b) DFT calculations comparing Ru<sub>2</sub>(chp)<sub>4</sub>O (**6**) in both singlet and triplet ground states were performed here. Results from both the BP86 and B3LYP functionals are in agreement that the favored electronic ground state for **6** is the singlet state. See [Supporting Information](#) for computational details.

(31) (a) Atkins, P. W.; Symons, M. C. R. *J. Chem. Soc.* **1962**, 4794. (b) Livingston, R.; Zeldes, H. *J. Chem. Phys.* **1964**, *41*, 4011. (c) Wertz, J. E.; Bolton, J. R. *Electron Spin Resonance: Elementary Theory and Practical Applications*; Chapman and Hall: New York, 1986; p 164.

(32) (a) Rotlevi, E.; Treinin, A. *J. Phys. Chem.* **1965**, *69*, 2645. (b) Svoboda, O.; Kubelová, L.; Slaviček, P. *J. Phys. Chem. A* **2013**, *117*, 12868.

(33) (a) Madsen, D.; Larsen, J.; Jensen, S. K.; Keiding, S. R.; Thøgersen, J. *J. Am. Chem. Soc.* **2003**, *125*, 15571. (b) Thøgersen, J.; Gadegaard, A.; Nielsen, J.; Jensen, S. K.; Petersen, C.; Keiding, S. R. *J. Phys. Chem. A* **2009**, *113*, 10488.

(34) Brown, T. R.; Dolinar, B. S.; Hillard, E. A.; Clérac, R.; Berry, J. F. *Inorg. Chem.* **2015**, *54*, 8571.

(35) Lutterman, D. A.; Degtyareva, N. N.; Johnston, D. H.; Gallucci, J. C.; Eglin, J. L.; Turro, C. *Inorg. Chem.* **2005**, *44*, 5388.

(36) Lin, C.; Ren, T.; Valente, E. J.; Zubkowski, J. D.; Smith, E. T. *Chem. Lett.* **1997**, *26*, 753.

(37) Stoll, S.; Schweiger, A. *J. Magn. Reson.* **2006**, *178*, 42.

(38) APEX2; Bruker-AXS, 2014.

(39) (a) SADABS 2014/5; Krause et al., 2014. (b) TWINABS 2012/1; Sheldrick, 2012.

(40) XS 2013/1; Sheldrick, 2013.